RESEARCH ARTICLE

ADVANCED
PHOTONICS
RESEARCH
Open Access

www.adpr-journal.com

Structural Integration of Carbazole and Tetraphenylethylene: Ultrafast Excited-State Relaxation Dynamics and Efficient Electroluminescence

Sarah K. M. McGregor, Chinju Govind, Michael K. R. Wood, Atul Shukla, Hyunsoo Lim, Romain J. Lepage, Elizabeth H. Krenske, Narayanan Unni K. N., Ayyappanpillai Ajayaghosh, Venugopal Karunakaran,* Ebinazar B. Namdas,* and Shih-Chun Lo*

The synthesis, characterization, and spectroscopic investigations of a new solution-processable N-styrylcarbazole-linked tetraphenylethylene (TPE) derivative (TPE-BCzS) are reported, exhibiting green–orange emission. While the material displays weak photoluminescence (PL) in solution with a low PL quantum yield (PLQY of $4 \pm 0.2\%$), significant PL enhancement in neat-film PLQY ($55 \pm 8\%$) is observed. Studies using steady-state spectroscopy, and femtosecond and nanosecond transient absorption spectroscopy reveal details of the excited-state dynamics, consisting of the Franck–Condon (FC) state, non-radiative conformational relaxation, and formation and decay of the triplet excited state generated via intersystem crossing (ISC) upon ultrafast photoexcitation. Solution-processed organic light-emitting diodes (OLEDs) based on TPE-BCzS display maximum external quantum efficiencies of 1.8% and 1.7% for neat and blend films (20 wt% in a 4,4′-bis(N-carbazolyl)-1,1′-biphenyl host), approaching the theoretical efficiency limit for the determined PLQYs of the films. While TPE materials are typically associated with aggregation-induced emission, it is reported that the enhanced PLQYs in the solid state are due to restriction of structural relaxations in the solid state and not due to the commonly misunderstood aggregation effect.

1. Introduction

Organic semiconducting materials have garnered substantial attention owing to their potential utility in applications such as organic light-emitting diodes (OLEDs), photovoltaic cells, organic field-effect transistors (OFETs), organic light-emitting transistors (OLETs),[1] and organic lasers.[2] Most conventional organic chromophores are highly luminescent in solution but unfortunately experience aggregation caused quenching (ACQ) in the solid state, whereby strong intermolecular π–π stacking gives rise to the formation of nonemissive species such as excimers and exciplexes.[3] ACQ can be suppressed by depositing the chromophores within a suitable host material, effectively separating and diluting the molecules to prevent the formation of nonemissive excited species, and/or by utilizing a dendritic structure where the emissive core is protected from core–core interactions through the attachment of bulky dendrons.[4] These

Dr. S. K. M. McGregor, M. K. R. Wood, A. Shukla, H. Lim,
Prof. E. B. Namdas, Prof. S.-C. Lo
Centre for Organic Photonics & Electronics
The University of Queensland
Brisbane, QLD 4072, Australia
E-mail: e.namdas@uq.edu.au; s.lo@uq.edu.au

Dr. S. K. M. McGregor, M. K. R. Wood, Dr. R. J. Lepage,
Prof. E. H. Krenske, Prof. S.-C. Lo
School of Chemistry and Molecular Biosciences
The University of Queensland
Brisbane, QLD 4072, Australia

C. Govind, Prof. N. U. K. N., Prof. A. Ajayaghosh, Prof. V. Karunakaran
Photosciences and Photonics Section
Chemical Sciences and Technology Division
CSIR-National Institute for Interdisciplinary Science and Technology
Trivandrum 695019, India
E-mail: k.venugopal@niist.res.in

A. Shukla, H. Lim, Prof. E. B. Namdas
School of Mathematics and Physics
The University of Queensland
Brisbane, QLD 4072, Australia

The ORCID identification number(s) for the author(s) of this article can be found under https://doi.org/10.1002/adpr.202000144.

**ADVANCED
SCIENCE NEWS**
www.advancedsciencenews.com

**ADVANCED
PHOTONICS
RESEARCH**
Open Access
www.adpr-journal.com

strategies have met with some success but adversely serve to increase the respective complexity in device fabrication, often leading to decreased charge-carrier mobility,[5] or require intensive material synthesis and purification. In contrast, aggregation-induced emission (AIE) is a phenomenon that provides enhanced photoluminescence (PL) upon aggregation of the lumiphore.[3] Typically, AIE materials possess highly twisted molecular conformations, where nonplanar configurations prevent intermolecular π–π interactions, circumventing decay by nonradiative pathways.[5a,6] Notably, AIE materials offer the potential of simplified OLED device architectures such as homojunctions as host materials are often not required to maintain high emission efficiencies. Despite the interest in AIE materials, understanding of the fundamental ultrafast relaxation processes responsible for the AIE phenomenon is yet to be established. Though molecular aggregation is perceived as the direct source of increased PL emission, this phenomenon is often misunderstood due to its interrelation with other structural effects such as restriction of intramolecular rotation and/or vibration twisted intramolecular charge transfer (TICT), as well as excited-state intramolecular proton transfer (ESIPT)[7]—all of which can lead to increased PL quantum yields (PLQYs) in the solid state.[8]

Some of the most widely investigated AIE chromophores are based on cyclopentadiene[9] and tetraphenylethylene (TPE). As a prototypical AIE chromophore, TPE and its derivatives have been extensively studied within the organic semiconductor field, as well as lately in sensing[10] and biological applications,[11] owing to their unique AIE behavior, facile synthesis, and ease of functionalization. Of particular interest is the decoration of the TPE core to maintain the desirable properties of the conventional chromophore, while imbuing it with AIE behavior to help tune emission properties such as the development of electrochromic materials with ultrahigh fluorescence contrast.[10d]

Carbazole is one such conventional chromophore, which is frequently used as a structural feature within efficient light-emitting compounds due to its excellent hole-transporting ability[12] and good thermal stability.[13] However, the rigid, planar geometry of carbazole and its derivatives tends to have strong intermolecular interactions in the solid state (even in solution in some cases),[14] leading to the detrimental ACQ.[12a] As a result, there have been a number of studies focused on developing carbazole-decorated TPE derivatives that retain the favorable thermal and hole-transporting properties of carbazole while eliminating the ACQ effect for OLEDs.[6,12a,15] The majority of the

work has relied on vacuum deposition of the TPE derivatives in OLED fabrication, including also the use of the TPE materials within a host matrix. Solution processing, on the contrary, offers cost-effective deposition techniques such as spin coating, inkjet printing, and slot-casting. Despite the benefits of the technique, to date, there have limited studies on solution-processed OLEDs utilizing nondoped AIE emitters.[16] Furthermore, understanding the fundamental ultrafast relaxation processes responsible for AIE is essential for new material design and device application.

In this work, we designed and synthesized a bis-decyloxy- and bis-carbazolylstyryl-functionalized TPE derivative, 1,2-bis(4-((E)-4-(9H-carbazol-9-yl)styryl)phenyl)-1,2-bis(4-decyloxy)phenyl)ethene (**TPE-BCzS**), with the intention of developing an AIE material with good charge-transporting properties and a high solid-state PLQY to be used in solution-processed OLEDs. Due to the complex nature of AIE, we sought to gain insights into the structural origin of the emissive species by extensively investigating the ultrafast excited-state relaxation dynamics of **TPE-BCzS** using steady-state and femtosecond pump–probe spectroscopy and nanosecond laser flash photolysis spectroscopy. We established that the enhancement of **TPE-BCzS** emission in the solid state is due to restriction of structural relaxations and not due to the commonly misunderstood aggregate effect.

2. Results and Discussion

2.1. Material Synthesis

The synthetic route to **TPE-BCzS** is shown in **Scheme 1**. The precursors 4-bromophenyl-4-hydroxyphenylmethanone[17] and 9-(4-vinylphenyl)-9H-carbazole[18] were prepared as per literature sources. Attachment of the solubilizing groups to 4-bromophenyl-4-hydroxyphenylmethanone was achieved by treatment with 1-bromodecane and potassium hydroxide in anhydrous dimethyl sulfoxide[19] to give **1** in an 80% yield. **1** was subjected to a McMurry coupling with zinc powder and titanium tetrachloride to give **2** (57%). The final step in the synthesis was a microwave-assisted Heck reaction with 9-(4-vinylphenyl)-9H-carbazole in the presence of palladium(II) acetate and tri-o-tolylphosphine in triethylamine to provide the target **TPE-BCzS** (53%) in 1:1 ratio of E/Z-TPE isomers as estimated from ^{1}H nuclear magnetic resonance (NMR) spectrum. While one
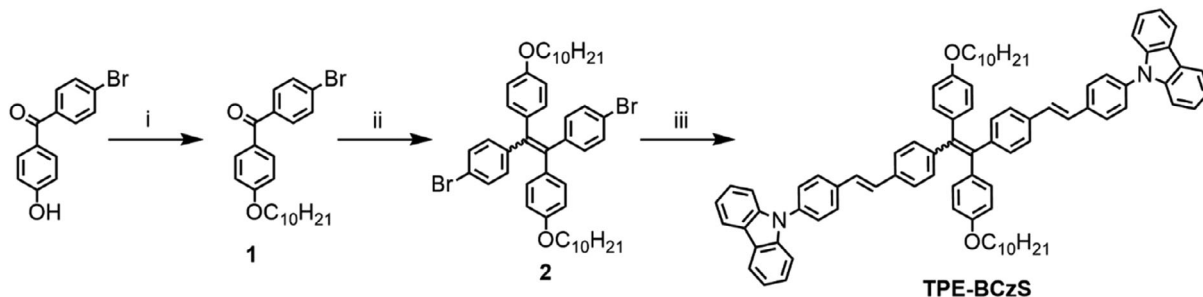
Scheme 1. Synthetic route to **TPE-BCzS**: i) 1-bromodecane, KOH, DMSO, r.t., 5 h (80%); ii) TiCl$_4$, Zn, THF, Ar$_{(g)}$, −78 °C, 30 min, reflux, 16 h (57%); iii) 9-(4-vinylphenyl)-9H-carbazole, Pd(OAc)$_2$, P(o-tol)$_3$, NEt$_3$, MW, 150 °C, 30 min (53%). DMSO, dimethyl sulfoxide; r.t., room temperature; THF, tetrahydrofuran; OAc, acetoxy; o-tol, o-tolyl; MW, microwave.

isomerically enriched sample was identified (details in the Supporting Information), all attempts to isolate pure samples of the two isomers were not successful due to the rapid equilibration toward a 1:1 E/Z mixture as observed upon dissolution in organic solvents. Thus, comparison of the two individual isomers in the context of solution-processed devices is not meaningful. It is assumed that all data collected from solution-processed samples of **TPE-BCzS** contain both E and Z isomers in approximately equal amounts. Moreover, due to the attachment of the two long solubilizing decyloxy groups, **TPE-BCzS** was found to have high solubility in most common organic solvents (e.g., dichloromethane, chloroform, THF, and toluene), enabling good film forming quality from spin coating. Details of the material synthesis and characterization data can be found in the Supporting Information.

2.2. Thermal Properties

The thermal properties of **TPE-BCzS** were studied using thermal gravimetric analysis (TGA) and differential scanning calorimetry (DSC). As commonly observed with materials featuring carbazole functional groups, **TPE-BCzS** exhibited excellent thermal stability with a decomposition temperature (T_d) (with a 5% weight loss) of 389 °C (Figure S2, Supporting Information). Figure S3 in Supporting Information shows the DSC heating trace at a scan rate of 200 °C min^{-1}. The melting point (mp) was detected in the first heating scan with a broad endothermic event centered at 156 °C, which matched closely with the large melting range of 155–175 °C observed with a traditional mp apparatus. Subsequent heating thermocycling showed the emergence of minor endothermic events spanning from 90 to 150 °C (Figure S3, Supporting Information). Explicit assignment of these transitions could not be achieved due to their low intensity and broad nature. However, they likely represent the glass transition temperatures (T_g) of the E and Z isomers and/or isomerization temperatures. To further investigate the E and Z isomers' influences on thermal behavior, a sample of **TPE-BCzS** containing the two isomers in an approximate ratio of 3:7 (as determined by relative integration of ^{1}H NMR peaks, albeit not explicitly assigned to the respective isomers; see Figure S4, Supporting Information) was subjected to DSC under identical conditions. As can be seen from Figure S3, Supporting Information, the isomerically enriched sample gave comparable results to that of the 1:1 mixture, suggesting isomeric purity does not significantly impact the thermal properties of the material. Recovery and ^{1}H NMR analysis of the thermocycled sample revealed that it became an approximate 1:1 mixture of E/Z isomers, confirming that the TPE isomerization temperature of **TPE-BCzS** occurs within the DSC scanning window. Moreover, the energy barrier of the isomerization can be overcome by purely thermal methods in the absence of light or solvent, as demonstrated by previous studies with TPE systems.[20]

2.3. Electrochemical Properties

The electrochemical properties of **TPE-BCzS** were investigated with cyclic voltammetry (CV) in dichloromethane and THF solutions for oxidation and reduction, respectively. The redox

Table 1. Thermal and electrochemical properties of **TPE-BCzS**.

	T_m [°C]	T_d [°C][a]	IP [eV][b]	EA [eV][b]	CV gap [eV][c]	E_g [eV][d]
TPE-BCzS	155–175	389	−5.3	−2.4	2.9	2.8

[a]Data acquired from TGA at 10 °C min^{-1}, with values corresponding to a 5% weight loss; [b]Estimated from CV and referenced to ferrocenium/ferrocene couple; [c]Calculated by the difference between the first oxidation and reduction half-wave potentials from the CV measurements; [d]Optical gap (E_g) estimated from the intersect of the normalized absorption and PL spectra in THF solution (Figure S10a, Supporting Information).

profiles (Figure S5, Supporting Information) exhibited high reversibility across multiple cycles in the respective solvents, indicating good stability of both radical cationic and radical anionic species under the conditions studied. **TPE-BCzS** was found to have first half-wave ($E_{1/2}$) oxidation and reduction potentials at ≈0.5 and −2.4 V, respectively, versus the ferrocenium/ferrocene couple. This gave an estimated ionization potential (IP) and electron affinity (EA) of −5.3 and −2.4 eV, respectively, by using ferrocene with a work function of ≈−4.8 eV versus vacuum level.[21] This further gave a calculated electrochemical gap of 2.9 eV, which is essentially close to that (2.8 eV) of the estimated optical gap from THF solution, as determined from the crossover of the absorption and PL spectra, using the method outlined by Lakowicz[22] (**Table 1**). Due to the rapid isomerization in solution as observed from the aforementioned ^{1}H NMR experiments, it is expected that there will be significant contributions from both Z and the E isomers of **TPE-BCzS** for these transitions. This is supported by the effectively identical values for the calculated molecular orbital energies of the two individual isomers (see Figure S6–S9, Supporting Information).

2.4. Density Functional Theory Calculations

To gain better understanding into the photophysical properties of **TPE-BCzS**, time-dependent density functional theory (TD-DFT) computations were conducted for both the E and Z isomers, using CAM-B3LYP-D3(BJ)/6-31+G(d,p) with an integral equation formalism polarizable continuum model (IEFPCM) representation of dichloromethane as the solvent. The n-decyloxy chains were modeled as methoxy groups. The optimized molecular geometries and frontier orbitals are shown in **Figure 1**. For both isomers, the highest occupied molecular orbital (HOMO) is distributed over the central TPE moiety and styryl-phenyl components. The carbazole units are twisted by 60° relative to the main conjugated backbone, and therefore, there is no significant contribution from the carbazoles to the HOMO. Instead, the carbazole moieties contribute to HOMO-1 and HOMO-2 (see the Supporting Information). The lowest unoccupied molecular orbital (LUMO) is primarily localized on the ethylene core and two attached phenyl-vinyl-phenyl moieties, which possess extended π-conjugation. Unlike the HOMO, there is no contribution from the anisole rings in the LUMO. It is important to note that there is a node between the carbons of the central double bond in the LUMO. This is consistent with the observations of rapid isomerization in solution as observed in ^{1}H NMR experiments such that population of the LUMO through either photoexcitation or charge injection in a device
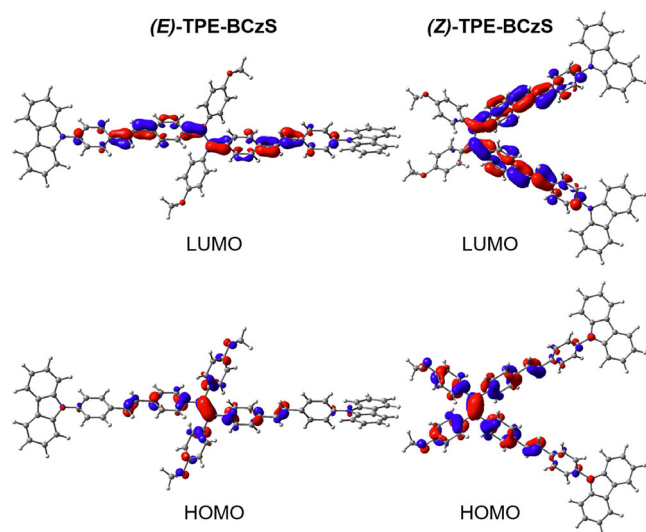
Figure 1. HOMO and LUMO of the *E* and *Z* isomers of a model of **TPE-BCzS**, calculated with CAM-B3LYP-D3(BJ)/6-31 + G(d,p) in dichloromethane. The decyloxy groups of **TPE-BCzS** have been replaced by methoxy groups in the model compound.

can result in a decrease in bond order of the central double bond, facilitating *E/Z* isomerization.

The calculated vertical excitation energies are in agreement with experimental photophysical results, with the predicted absorption maxima lying within 20–30 nm of experimental values (Figure S7, Supporting Information). The calculated absorption spectrum (in dichloromethane) indicated that the major transition at ≈390 nm is dominated by the *E* isomer and has HOMO → LUMO character, with a smaller contribution from the *Z* isomer. Conversely, the second peak at ≈360 nm is dominated by the HOMO →LUMO + 1 transition of the *Z* isomer, with a smaller contribution from the *E* isomer.

2.5. Steady-State Photophysics and Transient PL Spectroscopy

The steady-state photophysical properties of **TPE-BCzS** were studied in toluene solution, neat films, and blend films (20 wt% doped in CBP). **Figure 2**a shows the normalized absorption and
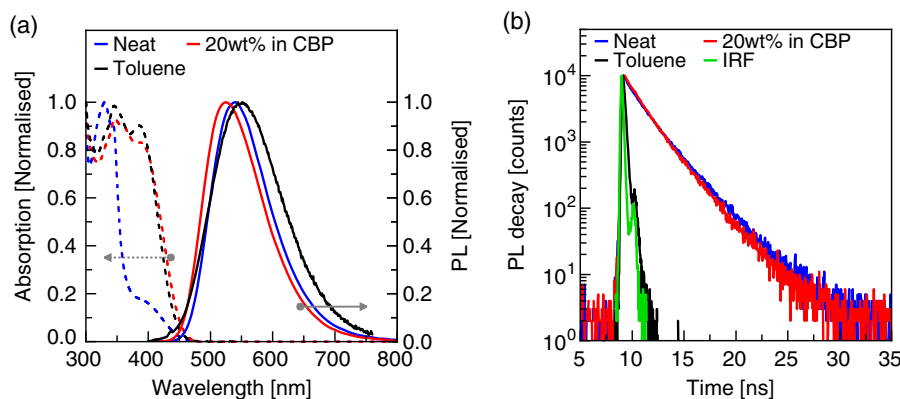
PL spectra. Compared with the sky-blue emission of the parent TPE molecule,[23] the introduction of bis-carbazolylstyryl units to **TPE-BCzS** causes a significant red-shift of both the absorption and PL spectra, with emission now falling within the green–orange region. Although minor, the solution PLQY of **TPE-BCzS** was also enhanced with a PLQY of 4% in toluene solution, compared with that (<1%) of the parent TPE.[23] The enhancement in solution PLQYs can be attributed to the introduction of π-conjugated carbazolylstyryl groups, where the increased molecular size and π-conjugation enhance the radiative rate constants and/or decrease the nonradiative losses. However, the presence of a large Stokes shift in **TPE-BCzS** clearly indicates that the absorptive species still undergoes significant structural changes prior to attaining the excited-state configuration with higher radiative coupling to the ground state. This reduction in nonradiative losses is also observed by the significant rise in PLQY (55%) and PL lifetime (1.9 ns) in the solid state (Figure 2b and **Table 2**).

To further confirm this, we performed steady-state photophysical properties of **TPE-BCzS** in solvents with differing polarity. Figure S10, Supporting Information, shows the absorption spectra, PL spectra, and TCSPC PL decay profiles in cyclohexane, toluene, 1,4-dioxane, THF, and ethyl acetate, with corresponding peak maxima and fluorescence lifetimes tabulated in Table S2, Supporting Information, in which TCSPC is time-correlated single photon counting. The absorption and PL spectra did not show any significant change with solvent polarity, indicating the large Stokes shifts do not arise from the intramolecular charge transfer (ICT) state. Moving from solution to solid state, the PLQYs of **TPE-BCzS** were observed to increase from 4% in toluene solution to 52% and 55% in the blend and neat films, respectively (Table 2). Furthermore, the lifetime obtained from solution is much shorter than that in the solid state (Table 2). Coupled with the hypsochromic shift in the PL (Figure 2) when moving to the solid state, this would suggest that the enhancement of PLQY in the solid state could be due to restriction of structural relaxations, not to an aggregation effect.

2.6. Ultrafast Pump–Probe Absorption Spectroscopy

To understand the excited state and structural relaxation dynamics of **TPE-BCzS**, femtosecond time-resolved transient

Figure 2. TPE-BCzS in toluene solution, neat film, and blend film (20 wt% in CBP). a) Normalized absorption and PL spectra ($\lambda_{ex} = 350$ nm). b) Comparison of PL decay, showing a clear enhancement in lifetime moving from solution to solid state.

Table 2. Photophysical properties of **TPE-BCzS** in toluene solution, neat, and blend (20 wt% in CBP) films, spin-coated from chloroform solution.

	λ_{PL} [nm]	PLQY [%]	τ_f [ns]	k_r [$\times 10^8$ s^{-1}]
Solution	544	4 ± 3	0.13	3.08
Blend film	525	52 ± 8	2.06[a]	2.72
Neat film	539	55 ± 7	1.91[a]	2.66

[a]Average lifetime.

absorption spectra were measured in toluene at room temperature by exciting at 385 nm. The transient absorption spectra of **TPE-BCzS** at various time delays are shown in **Figure 3**. Figure 3a shows the early spectral dynamics, where the negative change in absorbance in the region of 350–425 nm corresponds to the bleach band due to ground-state depopulation. The evolution of a peak at ≈470 nm is due to the excited-state absorption or the formation of new species (vide infra). The negative band at 490–525 nm is attributed to the stimulated emission (SE) band due to its characteristic red-shift with change in intensity resulting from solvation relaxation dynamics in the shorter time scales. Figure 3b shows the evolution from 6.15 to 83.15 ps, where the intensity of the negative SE band gradually decreases and is replaced by a positive transient absorption band at ≈585 nm. Intensification of absorption around 470 nm was also observed during these time scales. In Figure 3c, a decrease to the intensity of the bleach band and a decrease to the broad positive band stretching from 470 to 585 nm was observed with longer delay times, resulting in negligible absorption at 1.08 ns. Transient

absorption spectra of **TPE-BCzS** in toluene in the longer wavelength region from 525 to 750 nm are shown in Figure 3d–f. Short time scales from 0.20 to 3.00 ps are shown in Figure 3d, which features a broad excited-state absorption band centered at 740 nm. This excited-state absorption band continually decreases with time, with minimal absorbance remaining at 969.2 ps (Figure 3f). The longer wavelength region also shows the previously discussed peak at 585 nm, which has its strongest positive response at ≈85 ps, before gradually decreasing over longer time scales.

The data analysis of the femtosecond transient absorption spectra consisting of a 3D data set (wavelength, time, and change in absorbance) was performed with the global analysis program GLOTARAN.[24] It is known that the relaxation dynamics can only be described by multiexponential time constants due to overlap with other simultaneous processes of solvation dynamics, vibrational relaxation, and conformational relaxation. Therefore, four excited-state time constants, $\tau_1 = 2.36 \pm 0.2$ ps, $\tau_2 = 49.2 \pm 2.5$ ps, $\tau_3 = 157 \pm 7.5$ ps, and $\tau_4 \geq 1.2$ ns were optimally obtained to describe the relaxation dynamics of **TPE-BCzS** immediately after excitation. The long-lived component ($\tau_4 \geq 1.2$ ns) obtained from the femtosecond transient absorption spectra would not be accurate due to the limitation of the experimental setup, in which the translation delay generator can measure the delay time up to 1.7 ns (maximum). Therefore, we measured nanosecond transient absorption spectra of **TPE-BCzS**, using a nanosecond laser flash photolysis spectrometer.

As the SE near 490 nm obtained by exciting at 385 nm in toluene (Figure 3) shifts to the red region with increasing delay time, the fast component ($\tau_1 = 2.36$ ps) would correspond to solvation
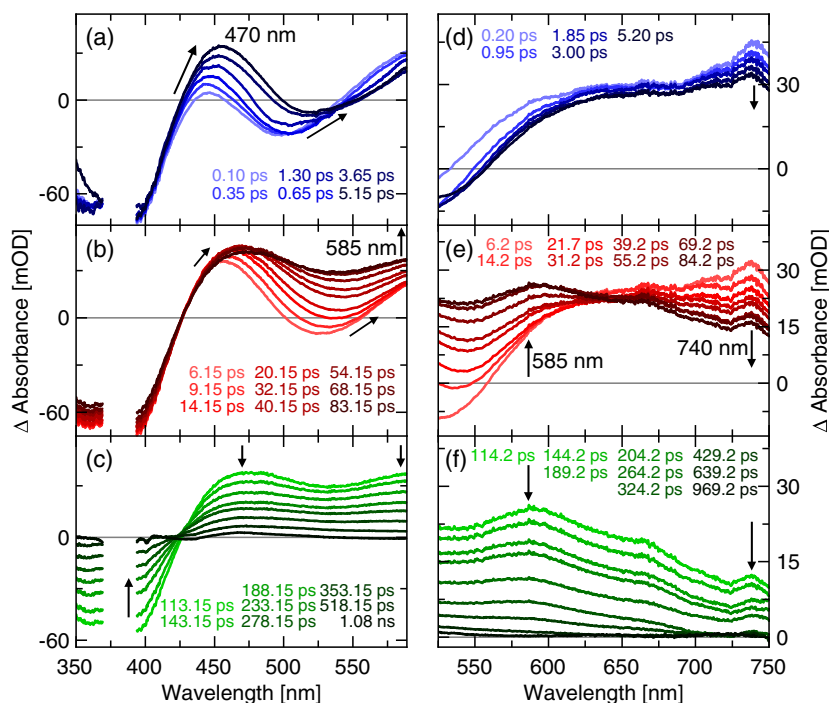

Figure 3. Femtosecond transient absorption spectra of **TPE-BCzS** in toluene with excitation at 385 nm in a–c, left) shorter wavelength region and d–f, right) longer wavelength region. Parts (a) and (d) show time scales between 0.1 and 5.2 ps; (b) and (e) between 6.1 and 85 ps; and (c) and (f) show longer time scales from 110 ps to 1.1 ns.

**ADVANCED
SCIENCE NEWS**

www.advancedsciencenews.com

**ADVANCED
PHOTONICS
RESEARCH**
Open Access

www.adpr-journal.com

relaxation processes from the Franck–Condon (FC) state to the solvent stabilized local excited state.[25] Conversely, this time constant may also correspond to intramolecular conformational changes,[25] emerging from the combination of elongation and partial twisting of the central C=C bond of the TPE moiety, occurring on the way from the FC geometry to the minimum energy geometry.[26] The second time constant ($\tau_2 = 49.2$ ps) would reflect the nonradiative conformational relaxation of central TPE unit.[23] As demonstrated through the computational calculations, the E and Z isomers of the central TPE core have extremely low energy differentials, which can subsequently lead to ultrafast nonradiative loss pathways. This is also consistent with the dramatic reduction in excited-state lifetime of sterically strained Z-stilbene ($\approx$1 ps), compared with that of E-stilbene ($\approx$100 ps) as reported in the literature.[27] This is followed by the transition from S_1 excited state in the form of SE and ISC with exponential decay kinetics of $\tau_3 = 157$ ps, which is further consistent with the TCSPC emission lifetime.

To gain insights into the long nanosecond excited-state decay component ($\tau_4 \geq 1.2$ ns), we performed nanosecond transient absorption spectroscopy using laser flash photolysis system by exciting at 355 nm in an inert atmosphere at room temperature. Figure S11, Supporting Information, shows the nanosecond transient absorption spectra of **TPE-BCzS** in toluene obtained at different delay times after laser excitation, with broad absorption maximum at $\approx$465 nm. The negative absorbance of the bleach band at 350 nm is attributed to the ground-state absorption of the compound. With increase in delay time, an overall decrease in absorbance is observed. The transient absorption spectra in toluene under both argon and oxygen-saturated atmospheres at $\approx$228 ns after laser irradiation are also shown in Figure S11, Supporting Information.

Compared with the argon-saturated environment, the peak at 465 nm is completely quenched by the presence of oxygen, indicating the broad signal arises from extremely oxygen sensitive triplet excited states of **TPE-BCzS**. It is noted that the transient absorption maximum at 465 nm is matching with the femtosecond transient absorption spectra. Figure S12, Supporting Information, shows the kinetic profile of **TPE-BCzS** probed at 465 nm in toluene under argon. A monoexponential fit was applied to the decay kinetics and the time constant for the triplet state was found to be 251 ns. Thus, the fourth time constant is attributed to the decay of the triplet excited state generated via ISC and can be conclusively seen in the nanosecond transient absorption spectroscopy (Figure 3 and Figure S11, Supporting Information). The resultant decay-associated spectra of **TPE-BCzS** in toluene are shown in Figure S13, Supporting Information.[28] A schematic representation of the four time constants of excited-state relaxation dynamics for **TPE-BCzS** is shown in **Figure 4** for clarity.

2.7. Electroluminescence and Charge Transport Properties

The emissive layer of OLEDs containing neat and doped **TPE-BCzS** (20 wt% in CBP) was fabricated using solution processing, where **Figure 5**a shows the OLED device structure and energy diagram of the materials. TPBi was chosen as the electron transport layer for easy electron injection to the emissive layer.
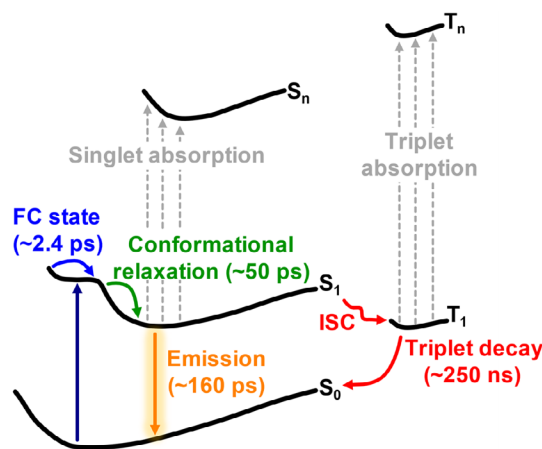

Figure 4. Schematic representation of excited-state dynamics of **TPE-BCzS**, showing the molecular transition leading to modulation in transient absorption traces. The four time constants were assigned to the FC state, nonradiative conformational relaxation, formation, and decay of triplet excited-state generated via ISC.

The current–density–voltage–luminance (J–V–L) curves for doped and nondoped OLEDs based on **TPE-BCzS** are shown in Figure 5b, with details of charge mobility (Figure S14, Supporting Information) in Section S5, Supporting Information. As shown in Figure 5c, the EQE of both devices approaches 2%, which can be compared with the expected maximum EQE of 2.5% of the material by having a solid-state PLQY of $\approx$50% (Table 2) and assuming 20% light outcoupling and singlet-to-triplet spin branching ratio of 1:3. The EL spectra of neat and blend films are almost identical (Figure 5d). This result is consistent with the previously discussed photophysical analysis, indicating the enhancement of **TPE-BCzS** emission in the solid state is due to restriction of rotation, and not due to the result of intermolecular aggregation. Full details of OLED device fabrication and characterization can be found in the Supporting Information.

3. Conclusions

The new TPE derivative, **TPE-BCzS**, reported here, facilitated a deeper understanding of the structural origin of emissive species commonly observed by TPE-based AIE materials. Based on the measurements using steady-state spectroscopy and femtosecond and nanosecond transient absorption spectroscopy, we observed four excited-state time constants ($\tau_1 = 2.36$ ps, $\tau_2 = 49.2$ ps, $\tau_3 = 157$ ps, and $\tau_4 = 251$ ns) to describe the ultrafast relaxation dynamics of **TPE-BCzS** immediately after ultrafast photoexcitation, involving FC state, nonradiative conformational relaxation, formation, and decay of triplet excited-state generated via ISC. Fabrication of OLEDs under both neat and blended architectures showed comparable device characteristics, where EQEs approached the theoretical maximum for the solid-state PLQYs. It was established that the observed enhancement of **TPE-BCzS** emission in solid state was due to restriction of structural relaxations and not due to intermolecular aggregation.
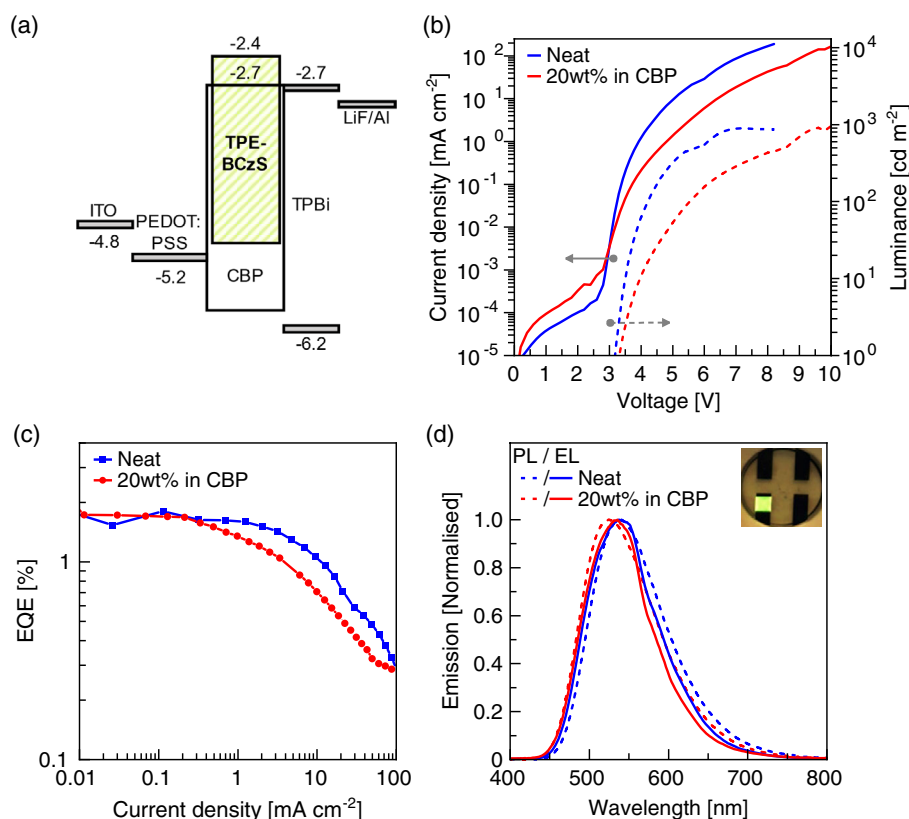
**ADVANCED
SCIENCE NEWS**

www.advancedsciencenews.com

**ADVANCED
PHOTONICS
RESEARCH**
Open Access

www.adpr-journal.com

Figure 5. Device characteristics for solution-processed **TPE-BCzS** in neat and doped (20 wt% in CBP) architectures, demonstrating a) energy levels of device structure, b) current–density–voltage–luminance (*J–V–L*) curves, c) EQE, and d) normalized PL and EL (at 10 mA cm^{-2}) spectra with inset of illuminated OLED device showing the emission pixel.

4. Experimental Section

General: All commercial reagents and chemicals were used as received unless otherwise noted.

Synthesis and Characterization: Tetrahydrofuran (THF) was dried using a vacuum–argon solvent purification system before use. Microwave reactions were conducted by using a CEM Discover-SP with closed vessels under dynamic control with a maximum power of 200 W and maximum pressure of 10 bar. Petroleum spirits with boiling point range 40–60 °C and dichloromethane were distilled under atmospheric pressure prior to use for column chromatography, using Merck LC60A 40–30 silica gel. Solvent ratio used for column chromatography is reported by volume. Melting points (mps) were measured in a glass capillary on a BÜCHI Melting Point B-545 with a heating rate of 5 °C min^{-1} and were quoted from the point of first melt to completely melted. TGA was conducted on a Perkin Elmer STA 6000 with scan rate 10 °C min^{-1} under continuous nitrogen flow and the TGA decomposition temperature was quoted at 5% weight loss. DSC was used to investigate thermal properties with heating and cooling rates of 200 °C min^{-1} under a nitrogen atmosphere with a Perkin Elmer Diamond DSC. High-resolution mass spectrometry (HRMS) was recorded on an Orbitrap Elite MS in positive mode. Details of the material synthesis and characterization can be found in the Supporting Information.

Electrochemical Measurements: Electrochemistry was performed on an Epsilon C3 BAS electrochemistry station using a glassy carbon and platinum working electrode for oxidation and reduction, respectively, a 0.1 M AgNO$_3$ acetonitrile solution reference electrode, and a platinum counter electrode with a scan rate of 100 mV s^{-1} to achieve reversible redox profiles. All measurements were completed at room temperature using 0.1 M

tetra-*n*-butylammonium perchlorate as the electrolyte. All solutions were purged with argon where sample concentration was ≈1 mM in dichloromethane (distilled from calcium hydride) and doubly distilled THF (from sodium and then lithium aluminum hydride) for oxidation and reduction, respectively. For all measurements, the ferrocenium/ferrocene (Fc$^+$/Fc) couple was used as the standard and in all cases several scans were completed to confirm the chemical reversibility of the redox processes.

Photophysical Measurements: UV–vis absorption spectra were recorded on a Varian Cary-5000 UV–vis spectrophotometer in 10 × 10 mm quartz cuvettes. Fluorescence spectra were measured using Jobin-Yvon Horiba Fluoromax 4 in steady-state mode using a xenon lamp as the excitation source. Solution PLQYs were determined by relative method with quinine sulfate as the reference (0.1 M in H$_2$SO$_4$, PLQY = 55%). All solutions were prepared in distilled toluene with a fixed optical density of ≈0.1 at the excitation wavelength of 350 nm. Solid-state PLQY measurements were performed using a calibrated integrating sphere.[29] All the samples were excited at 325 nm using HeCd Laser (IK series, Kimmon). TCSPC measurements were performed using FS5 fluorescence spectrometer (Edinburgh Instruments) with laser diode (375 nm) as the excitation source and emission was monitored at the peak of the fluorescence spectrum.

Femtosecond Transient Absorption Spectroscopy: The instrumentation details for the femtosecond transient absorption measurements have been described elsewhere.[30] It consists of a Ti:sapphire laser (MaiTai HP, Spectra Physics, USA) having a central wavelength of 800 nm with 80 MHz repetition rate and a pulse width of <100 fs. The amplified laser was split into two and the high energy beam was used as the pump (385 nm) for exciting the sample by using TOPAS (Prime, Light Conversion). The other part of the amplified beam (200 mW) focused on

**ADVANCED
SCIENCE NEWS**

www.advancedsciencenews.com

**ADVANCED
PHOTONICS
RESEARCH**
Open Access

www.adpr-journal.com

a 1 mm-thick CaF_2 plate to generate white light continuum (340–1000 nm) which further split into two beams (sample and reference probe beams). The sample cell (0.4 mm path length) was refreshed each time by rotating at a constant speed. Finally, the white light continuum was focused into a 100 μm optical fiber coupled to imaging spectrometer after passing through the sample cell. The transient absorption spectra were obtained by averaging about 2000 excitation pulses for each spectral delay. All the measurements were conducted at the magic angle (54.7°). All the transient absorption spectra obtained from the equipment are compensated for chirp of the white light by determining the time zero using coherent artifact observed in the solvent.[31] The time resolution of the pump–probe spectrometer is found to be about ≤ 120 fs. The integrity of the sample is tested by measuring the absorption spectra of the sample before and after the experiments and found to be no significant changes in the absorption spectra.

Nanosecond Transient Absorption Spectra: Nanosecond laser flash photolysis experiments were performed by exciting the samples with the third harmonic (355 nm) from an INDI-40-10-HG Quanta Ray Nd:YAG laser and using a kinetic spectrometer (LKS 60, Applied Photophysics). A 150 W pulsed xenon arc lamp was used as probing light source. The probe light transmitted through a sample in a 1 cm quartz cuvette was dispersed by a monochromator and detected by a photomultiplier tube coupled to a digital oscilloscope (Agilent Infiniium DSO8064A, 600 MHz, 4 GSa s^{-1}). The probe and laser beams were fixed at right angles to each other. The power of each laser pulse was monitored using a fast silicon photodiode (bypath). Solutions for laser flash photolysis studies were deaerated by purging with argon at least for 40 min before the experiments. All the experiments were conducted at room temperature.

Computational Studies: Computations were performed in Gaussian 16.[32] For computational efficiency, the calculations used a model of **TPE-BCzS**, in which the decyloxy groups were replaced by OMe groups. Geometries of the E and Z isomers of the model **TPE-BCzS** were optimized with CAM-B3LYP-D3(BJ)/6-31 + G(d,p) using an IEFPCM representation of dichloromethane as the solvent.[33] The ultrafine integration grid was used and the 2-electron integral accuracy was set to 10^{-14}. Vertical excitation energies were computed at the same level of theory, using the corrected linear response model of nonequilibrium solvation for excited states.[34]

Thin Film Preparation: Neat and blend films in all cases were spin-coated from toluene and chloroforms solutions, respectively. For photophysical measurements, samples were spin-coated onto fused silica substrates at 2000 rpm from 20 mg mL^{-1} solutions. Substrates were cleaned with sequential ultrasound sonication with acetone, isopropyl alcohol, and deionized water, followed by oxygen plasma treatment for 30 min to remove any organic impurities. Films with thickness of 80 and 100 nm were obtained for neat and blend films, respectively, as measured using Bruker Dektak XT profilometer.

Device Fabrication: On patterned indium tin oxide (ITO) substrates (of thickness 100 nm), poly(3,4-ethylenedioxythiophene)–poly(styrene-sulfonate) (PEDOT:PSS, AI4083) was filtered through a 0.45 μm syringe filter and spin-coated at 5000 rpm for 1 min, followed by thermal annealing at 130 °C for 20 min in air to produce a film of ≈ 30 nm. The substrates were transferred to a nitrogen glove box with oxygen and water levels <1 ppm. The emissive layer solution containing **TPE-BCzS** in chloroform (5 mg mL^{-1}) was filtered through 0.22 μm syringe filter and spin-coated on the PEDOT:PSS substrates at 3000 rpm for neat film (40 nm), and 1500 rpm for blended films (63 nm), containing 20 wt% in 4,4′-bis(carbazolyl)biphenyl (CBP). After deposition of films, the substrates were dried on a hotplate at 50 °C before transferring into a vacuum chamber, where 50 nm of 2,2′,2″-(1,3,5-benzinetriyl)tris(1-phenyl-1H-benzimidazole) (TPBi), 1 nm of LiF, and 100 nm of Al were sequentially deposited by thermal evaporation under vacuum ($\approx 10^{-7}$ Torr). The device current–voltage–luminesce and external quantum efficiency (EQE) characteristics were measured by a Hamamatsu system (C9920-12) under a nitrogen atmosphere without exposure to air.

Supporting Information

Supporting Information is available from the Wiley Online Library or from the author.

Conflict of Interest

The authors declare no conflict of interest.

Data Availability Statement

Data sharing is not applicable to this article as no new data were created or analyzed in this study.

[1] a) F. Cicoira, C. Santato, *Adv. Funct. Mater.* **2007**, *17*, 3421; b) C. Zhang, P. Chen, W. Hu, *Small* **2016**, *12*, 1252; c) C.-F. Liu, X. Liu, W.-Y. Lai, W. Huang, *Adv. Mater.* **2018**, *30*, 1802466; d) M. U. Chaudhry, K. Muhieddine, R. Wawrzinek, J. Sobus, K. Tandy, S.-C. Lo, E. B. Namdas, *Adv. Funct. Mater.* **2020**, *30*, 1905282.

[2] a) I. D. W. Samuel, G. A. Turnbull, *Chem. Rev.* **2007**, *107*, 1272; b) V. T. N. Mai, V. Ahmad, M. Mamada, T. Fukunaga, A. Shukla, J. Sobus, G. Krishnan, E. G. Moore, G. G. Andersson, C. Adachi, E. B. Namdas, S.-C. Lo, *Nat. Commun.* **2020**, *11*, 5623; c) Y. Jiang, Y.-Y. Liu, X. Liu, H. Lin, K. Gao, W.-Y. Lai, W. Huang, *Chem. Soc. Rev.* **2020**, *49*, 5885.

[3] J. Mei, N. L. C. Leung, R. T. K. Kwok, J. W. Y. Lam, B. Z. Tang, *Chem. Rev.* **2015**, *115*, 11718.

[4] a) S. Chénais, S. Forget, *Polym. Int.* **2012**, *61*, 390; b) S. Setayesh, A. C. Grimsdale, T. Weil, V. Enkelmann, K. Müllen, F. Meghdadi, E. J. W. List, G. Leising, *J. Am. Chem. Soc.* **2001**, *123*, 946.

[5] a) Z. Zhao, J. W. Y. Lam, B. Z. Tang, *J. Mater. Chem.* **2012**, *22*, 23726; b) Y. Liu, S. Chen, J. W. Y. Lam, P. Lu, R. T. K. Kwok, F. Mahtab, H. S. Kwok, B. Z. Tang, *Chem. Mater.* **2011**, *23*, 2536.

[6] Z. Zhao, C. Y. K. Chan, S. Chen, C. Deng, J. W. Y. Lam, C. K. W. Jim, Y. Hong, P. Lu, Z. Chang, X. Chen, P. Lu, H. S. Kwok, H. Qiu, B. Z. Tang, *J. Mater. Chem.* **2012**, *22*, 4527.

[7] S. Park, O.-H. Kwon, S. Kim, S. Park, M.-G. Choi, M. Cha, S. Y. Park, D.-J. Jang, *J. Am. Chem. Soc.* **2005**, *127*, 10070.

[8] a) Z. He, C. Ke, B. Z. Tang, *ACS Omega* **2018**, *3*, 3267; b) J. Mei, Y. Hong, J. W. Y. Lam, A. Qin, Y. Tang, B. Z. Tang, *Adv. Mater.* **2014**, *26*, 5429.

[9] S. Yin, Y. Yi, Q. Li, G. Yu, Y. Liu, Z. Shuai, *J. Phys. Chem. A* **2006**, *110*, 7138.

[10] a) H.-Q. Peng, X. Zheng, T. Han, R. T. K. Kwok, J. W. Y. Lam, X. Huang, B. Z. Tang, *J. Am. Chem. Soc.* **2017**, *139*, 10150; b) N. Sun, K. Su, Z. Zhao, Y. Yu, X. Tian, D. Wang, X. Zhao, H. Zhao, C. Chen, *ACS Appl. Mater. Interfaces* **2018**, *10*, 16105; c) N. Sun, K. Su, Z. Zhao, X. Tian, D. Wang, N. Vilbrandt, A. Fery, F. Lissel, X. Zhao, C. Chen, *J. Mater. Chem. C* **2019**, *7*, 9308; d) N. Sun, K. Su, Z. Zhou, D. Wang, A. Fery, F. Lissel, X. Zhao, C. Chen, *Macromolecules*, **2020**, *53*, 10117.

[11] a) W. Xu, D. Wang, B. Z. Tang, *Angew. Chem., Int. Ed.* **2020**, https://doi.org/10.1002/anie.202005899; b) Z. Zhao, C. Chen, W. Wu, F. Wang, L. Du, X. Zhang, Y. Xiong, X. He, Y. Cai, R. T. K. Kwok, J. W. Y. Lam, X. Gao, P. Sun, D. L. Phillips, D. Ding, B. Z. Tang, *Nat. Commun.* **2019**, *10*, 768.

[12] a) H. Shi, M. Li, L. Fang, X. Dong, X. Zhang, H. Peng, S. Chen, B. Z. Tang, *Synth. Met.* **2016**, *220*, 356; b) D. Meunmart, N. Prachumrak, T. Keawin, S. Jungsuttiwong, T. Sudyoadsuk, V. Promark, *Tetrahedron Lett.* **2012**, *53*, 3615.

[13] a) Z. Yang, Z. Chi, L. Zhou, X. Zhang, M. Chen, B. Xu, C. Wang, Y. Zhang, J. Xu, *Opt. Mater.* **2009**, *32*, 398; b) K. Yoshida, H. Nakanotani, C. Adachi, *Org. Electron.* **2016**, *31*, 287.

[14] S.-C. Lo, E. B. Namdas, C. P. Shipley, J. P. J. Markham, T. D. Anthopolous, P. L. Burn, I. D. W. Samuel, *Org. Electron.* **2006**, *7*, 85.

[15] a) Z. Zhao, P. Lu, J. W. Y. Lam, Z. Wang, C. Y. K. Chan, H. H. Y. Sung, I. D. Williams, Y. Ma, B. Z. Tang, *Chem. Sci.* **2011**, *2*, 672; b) J. Huang, X. Yang, J. Wang, C. Zhong, L. Wang, J. Qin, Z. Li, *J. Mater. Chem.* **2012**, *22*, 2478; c) H. Shi, Z. Gong, D. Xin, J. Roose, H. Peng, S. Chen, J. W. Y. Lam, B. Z. Tang, *J. Mater. Chem. C* **2015**, *3*, 9095.

[16] a) X. Zhou, Y. Xiang, F. Ni, Y. Zou, Z. Chen, X. Yin, G. Xie, S. Gong, C. Yang, *Dyes Pigm.* **2020**, *176*, 108179; b) F. Tang, J. Peng, R. Liu, C. Yao, X. Xu, L. Li, *RSC Adv.* **2015**, *5*, 71419; c) Q. Sun, X. Qiu, Y. Lu, X. Xu, H. Wang, S. Xue, W. Yang, *J. Mater. Chem. C* **2017**, *5*, 9157; d) D. Liu, J. Y. Wei, W. W. Tian, W. Jiang, Y. M. Sun, Z. Zhao, B. Z. Tang, *Chem. Sci.* **2020**, *11*, 7194; e) M. Li, F. Peng, L. Ying, J. Xu, *J. Mater. Chem. C* **2019**, *7*, 3553; f) D. Lo, C.-H. Chang, G. Krucaite, D. Volyniuk, J. V. Grazulevicius, S. Grigalevicius, *J. Mater. Chem. C* **2017**, *5*, 6054; g) F. Rizzo, F. Cucinotta, *Isr. J. Chem.* **2018**, *58*, 874.

[17] H. Dehmlow, J. D. Aebi, S. Jolidon, Y.-H. Ji, E. M. von der Mark, J. Himber, O. H. Morand, *J. Med. Chem.* **2003**, *46*, 3354.

[18] a) I. V. Vasilenko, A. A. Vaitusionak, J. Sutaite, A. Tomkeviciene, J. Ostrauskaite, J. V. Grazulevicius, S. V. Kostjuk, *Polymer* **2017**, *129*, 83; b) V. T. N. Mai, A. Shukla, A. M. C. Senevirathne, I. Allison, H. Lim, R. J. Lepage, S. K. M. McGregor, M. Wood, T. Matsushima, E. G. Moore, E. H. Krenske, A. S. D. Sandanayaka, C. Adachi, E. B. Namdas, S.-C. Lo, *Adv. Opt. Mater.* **2020**, *8*, 2001234.

[19] A. Shukla, N. R. Wallwork, X. Li, J. Sobus, V. T. N. Mai, S. K. M. McGregor, K. Chen, R. J. Lepage, E. H. Krenske, E. G. Moore, E. B. Namdas, S.-C. Lo, *Adv. Opt. Mater.* **2020**, *8*, 1901350.

[20] J. Wang, J. Mei, R. Hu, J. Z. Sun, A. Qin, B. Z. Tang, *J. Am. Chem. Soc.* **2012**, *134*, 9956.

[21] a) B. W. D'Andrade, S. Datta, S. R. Forrest, P. Djurovich, E. Polikarpov, M. E. Thompson, *Org. Electron.* **2005**, *6*, 11; b) S.-C. Lo, R. E. Harding, C. P. Shipley, S. G. Stevenson, P. L. Burn, I. D. W. Samuel, *J. Am. Chem. Soc.* **2009**, *131*, 16681.

[22] J. R. Lakowicz, *Principles of Fluorescence Spectroscopy*, 3rd ed., Springer-Verlag, New York **2006**.

[23] S. Kayal, K. Roy, S. Umapathy, *J. Chem. Phys.* **2018**, *148*, 024301.

[24] R. P. Chalmers, *J. Stat. Soft.* **2012**, *48*, 1.

[25] H. Zhu, M. Li, J. Hu, X. Wang, J. Jie, Q. Guo, C. Chen, A. Xia, *Sci. Rep.* **2016**, *6*, 24313.

[26] Y. Cai, L. Du, K. Samedov, X. Gu, F. Qi, H. H. Y. Sung, B. O. Patrick, Z. Yan, X. Jiang, H. Zhang, J. W. Y. Lam, I. D. Williams, D. Lee Phillips, A. Qin, B. Z. Tang, *Chem. Sci.* **2018**, *9*, 4662.

[27] a) A. L. Dobryakov, I. Ioffe, A. A. Granovsky, N. P. Ernsting, S. A. Kovalenko, *J. Chem. Phys.* **2012**, *137*, 244505; b) S. Abrash, S. Repinec, R. M. Hochstrasser, *J. Chem. Phys.* **1990**, *93*, 1041; c) R. J. Sension, S. T. Repinec, A. Z. Szarka, R. M. Hochstrasser, *J. Chem. Phys.* **1993**, *98*, 6291.

[28] a) D. Liu, A. M. El-Zohry, M. Taddei, C. Matt, L. Bussotti, Z. Wang, J. Zhao, O. F. Mohammed, M. D. Donato, S. Weber, *Angew. Chem., Int. Ed.* **2020**, *59*, 11591; b) X. Zhang, A. Elmali, R. Duan, Q. Liu, W. Ji, J. Zhao, C. Li, A. Karatay, *Phys. Chem. Chem. Phys.* **2020**, *22*, 6376.

[29] N. C. Greenham, I. D. W. Samuel, G. R. Hayes, R. T. Phillips, Y. A. R. R. Kessener, S. C. Moratti, A. B. Holmes, R. H. Friend, *Chem. Phys. Lett.* **1995**, *241*, 89.

[30] V. Karunakaran, *ChemPhysChem* **2015**, *16*, 3974.

[31] U. Megerle, I. Pugliesi, C. Schriever, C. F. Sailer, E. Riedle, *Appl. Phys. B* **2009**, *96*, 215.

[32] M. J. Frisch, G. W. Trucks, H. B. Schlegel, G. E. Scuseria, M. A. Robb, J. R. Cheeseman, G. Scalmani, V. Barone, G. A. Petersson, H. Nakatsuji, X. Li, M. Caricato, A. V. Marenich, J. Bloino, B. G. Janesko, R. Gomperts, B. Mennucci, H. P. Hratchian, J. V. Ortiz, A. F. Izmaylov, J. L. Sonnenberg, D. Williams-Young, F. Ding, F. Lipparini, F. Egidi, J. Goings, B. Peng, A. Petrone, T. Henderson, D. Ranasinghe, et al., in *Gaussian 16 Rev. B.01*, Gaussian, Inc., Wallingford, CT **2016**.

[33] a) T. Yanai, D. P. Tew, N. C. Handy, *Chem. Phys. Lett.* **2004**, *393*, 51; b) S. Grimme, J. Antony, S. Ehrlich, H. Krieg, *J. Chem. Phys.* **2010**, *132*, 154104; c) S. Grimme, S. Ehrlich, L. Goerigk, *J. Comput. Chem.* **2011**, *32*, 1456; d) J. Tomasi, B. Mennucci, R. Cammi, *Chem. Rev.* **2005**, *105*, 2999.

[34] M. Caricato, B. Mennucci, J. Tomasi, F. Ingrosso, R. Cammi, S. Corni, G. Scalmani, *J. Chem. Phys.* **2006**, *124*, 124520.

2000144 (9 of 9)